Labyrinthine instabilities of miscible magnetic fluids in a rotating Hele-Shaw cell

Cite as: Phys. Fluids **29**, 024109 (2017); https://doi.org/10.1063/1.4976720
Submitted: 12 September 2016 . Accepted: 03 February 2017 . Published Online: 27 February 2017

Mei-Yu Chen, Li-Que Chen, Huanhao Li, and Chih-Yung Wen

Labyrinthine instabilities of miscible magnetic fluids in a rotating Hele-Shaw cell

Mei-Yu Chen,[1] Li-Que Chen,[1] Huanhao Li,[2] and Chih-Yung Wen[2,a)]
[1]*Department of Aeronautics and Astronautics, National Cheng Kung University, Tainan 701, Taiwan*
[2]*Department of Mechanical Engineering, The Hong Kong Polytechnic University, Kowloon, Hong Kong*

(Received 12 September 2016; accepted 3 February 2017; published online 27 February 2017)

This study presents the first experimental results of confining miscible magnetic fluids in a rotating Hele-Shaw cell. Variations in the prominence of labyrinthine instabilities are observed under a range of experimental conditions, with different magnetic field strengths, gap depths, and rotation speeds. These instabilities are characterized by two modified Péclect numbers, namely, Pe_m (the ratio of the characteristic magnetic advection rate and the diffusion rate) and Pe_c (the ratio of characteristic rotation advection and the diffusion rate). The magnetic effect is characterized by dipolar repulsion, which triggers a distinctive fingering pattern differing from the progressive diffusion pattern that occurs without magnetic fields or rotation. Under the same rotation speed, the magnetoviscous effect will hinder the growth rate of the magnetic drops at the later stage. However, both the rotation effect and the gap depth greatly enhance the growth rate of the magnetic drops, as these conditions help to intensify the labyrinthine instabilities. In contrast, the countering pressure gradient produces an opposite force that constrains the trend toward expansion. Two major phases in the growth of instabilities are defined: a magnetization phase and a rotation phase, which are dominated by the magnetic and the rotation effect, respectively. The significance of the rotation effect is confirmed by the linear regression between the rotation growth rate and Pe_c. Finally, main fingering structures that evolve from the secondary waves are verified as having a wavelength λ to gap depth h relation of $\lambda \approx (7 \pm 1)\, h$. *Published by AIP Publishing.* [http://dx.doi.org/10.1063/1.4976720]

I. INTRODUCTION

Magnetic fluids are colloidal liquids consisting of magnetic nanoparticles suspended in non-magnetic carrier fluids. The amazing combination of fluidity and magnetic properties in such liquids has attracted significant interest from scholars and engineers.[1–6] If magnetic fluids are confined in a Hele-Shaw cell with a narrow gap between two parallel plates, labyrinthine instabilities (also called fingering instabilities) develop in the interfacial regions between the magnetic fluids and the surrounding fluids. When subjected to a normal external magnetic field, the repelling interaction of magnetic dipolar moments becomes much more significant within the Hele-Shaw cell, because the superparamagnetic nanoparticles within the magnetic fluids are always aligned with the direction of the external magnetic field. The major focus of attention has been on labyrinthine instabilities developed between magnetic fluids and their surrounding fluids, either immiscible or miscible.

Labyrinthine instabilities on immiscible interfaces are usually investigated by examining cases in which a sharp, well-defined interface is established by the magnetic fluids, without mixing with the surrounding non-magnetic fluids. However, recent theoretical analyses[7] and intensive numerical simulations[8–13] have highlighted the equally important and highly interesting labyrinthine instability that can be found at miscible interfaces, in cases where the interfacial surface tension is absent and the diffusive effect predominates instead. Due to the diffusive nature of miscible interfaces, we represent the degree of miscible labyrinthine instability by a magnetic Péclect number (the ratio of characteristic diffusion time to characteristic magnetic advection time) rather than by a magnetic Bond number (the ratio of characteristic magnetic force to surface tension). Igonin and Cebers[7] conducted a linear stability analysis of both a sharp interface and a diffused interface, and established a parallel between the approaches based on Darcy's law and those based on the Brinkman equations. Chen and Wen[8] used numerical simulations to reveal that the original circular droplets of miscible magnetic flows in a radial Hele-Shaw cell can extend intensive fingerings under conditions involving high-intensity magnetic parameters and viscous contrast. The prominence of these fingerings was analyzed under various control parameters, including the Pe_h, a modified magnetic Péclect number, the viscosity contrast, and various convective effects. Numerical simulations with a high order of accuracy were performed by Chen[9] and Hu and Joseph,[14] who discovered that the results for miscible magnetic flows were qualitatively similar to the experimental results for immiscible magnetic flows when considering the effects of Korteweg stresses.

Nevertheless, compared with the thorough investigations that have been conducted on immiscible situations, these studies of miscible flows are clearly incomplete. This lack of detailed experimental research is due to the difficulties caused by transient diffusive effects in miscible interfaces. In contrast to the homogeneous fields of viscosity and magnetization in

a)Author to whom correspondence should be addressed. Electronic mail: cywen@polyu.edu.hk

well-defined immiscible domains, the diffusive effects of miscible interfaces lead to transient and non-uniform distributions of viscosity and magnetization in the mixing regions of miscible fluids. Without detailed experimental investigations, the theoretical models and the numerical simulations conducted on these fluids cannot be verified.

Wen *et al.*[13] executed the first experiment on the labyrinthine instability of miscible and immiscible magnetic drops, and found a consistent trend of quantitative growth in the interfacial length, which supported the previous numerical results.[9,11] Wen[15] also conducted a series of systematic experiments that revealed the formation of a secondary wave of miscible magnetic fluids, caused by the three-dimensional factor of gap depth h, which had never been observed or simulated previously. Wen's study confirmed the limitations of the conventional two-dimension theoretical model, which did not consider the gap depth h. In addition, Wen observed that the interfacial length grew continuously in the early phase of the process, but began to decline when the magnetic field reached the preset value, consistent with the observations made by Cebers's group.[16,17] The growth rate in the early phase was in linear proportion to $(dH/dt)^{1/2}$ and $h^{3/2}$, where dH/dt was the sweep rate of the magnetic field. Therefore, the degrees of facilitation induced by the sweep rate and three-dimensional effect could be verified.[24]

In addition to the studies focused on stationary Hele-Shaw cell systems, rotating Hele-Shaw cell systems have been subjected to intensive investigations.[10,18–26] These rotating systems have attracted interest due to their potential applications in tasks such as spin-coating, mixing and cleaning with organic solvents, or biomedical separations. According to the computational studies performed by Schwarz,[19] fingerings tend to extend with the passing of time in a rotating Hele-Shaw cell two-phase flow. More accurate results were obtained by applying the modification developed by Waters and Cummings.[18] Chen and Wang[22] modeled miscible flows in a rotating Hele-Shaw cell by means of a highly accurate numerical scheme. These researchers found that under conditions where the central density and the viscosity of the fluids were higher, the centrifugal force competed with both the viscous force and diffusion to drive the instability. Waters and Cummings[18] theoretically discussed the mechanism by which the Coriolis effect induces tiny fingerings to grow backwards, against the rotational flow in the Hele-Shaw cell. Chen[10] conducted a numerical examination, and found that a stronger Coriolis effect could easily stabilize the miscible interface without additional injection. However, few studies have examined miscible magnetic fluids in rotating Hele-Shaw cells.

Notably, the viscosity of magnetic fluids changes according to the strength of the magnetic field. Li[27] reported that the viscosity of magnetic fluids was much greater in the direction perpendicular to the external magnetic field than in the direction of the applied field, due to the anisotropy of magnetic fluids. McTague[28] found that the viscosity of magnetic fluids became greater as the external magnetic field grew stronger, describing this effect as a magnetoviscous effect. Further observations of the changes in the viscosity of magnetic fluids in relation to external magnetic fields have made important contributions to understanding labyrinthine instability.

In this study, we present a systematic experimental analysis of the miscible labyrinthine instabilities of magnetic flows in a rotating Hele-Shaw cell. Two major modified Péclect numbers are defined to evaluate the labyrinthine instabilities and the growth of magnetic drops in fluids confined by a rotating Hele-Shaw cell under various experimental settings. Four major factors affecting the instabilities of these fluids are systematically and experimentally studied: the strength of magnetic fields, rotation speeds, gap depths, and the effects of countering pressure gradients.

This study is presented in three major sections. Following the introduction in Section I, Section II describes the experimental setup and design. Section III reports the results of the experiments and the relevant analyses, including discussions of the global flow and interfacial features. The analysis in Subsection III A focuses on the morphology of global flow visualization and the pattern of interfacial instabilities. Sub-Section III B examines the growth rates of the magnetic drops, as illustrated by a set of growth curves, and analyzes various physical effects of the instabilities. Finally, the conclusions from the investigation are drawn in Section IV.

II. EXPERIMENTAL SETUP

The experimental equipment illustrated in Fig. 1(a) is a modification of the setup used in Wen's previous study.[15] The Hele-Shaw cell is defined by two parallel plates with a narrow gap, h, where a magnetic drop with an initial radius of R_0 = 7.5 mm and its surrounding miscible fluids are confined. The rotation system is connected to the Hele-Shaw cell by a belt, so that the rotational motion of the Hele-Shaw cell can be accurately controlled by adjusting the voltage of a DC motor. The uniform perpendicular magnetic field strength, H, is induced by a pair of Helmholtz coils within R = 60 mm. The coils are immersed in a water box to keep the temperature constant at 27 °C and to stabilize the uniformity of the magnetic field. The magnetic field strength can be adjusted by a power supplier, and is measured with a Gauss meter (Kantec Model TM-701). For better visualization of the interfacial morphologies of the magnetic drop, the upper plate of the Hele-Shaw cell is made of transparent acrylic with a 10 mm thickness, and the lower plate is made of opaque white acrylic with a 14 mm thickness. A circular groove is cut under the surface of the lower plate, as shown in the upper right image in Fig. 1(b), to ensure the outer fluid can be made to flow in a circular motion for the open-flow case.

The magnetic fluids used in the experiments are commercial light mineral oil-based ferrofluids (EMG 905), produced by the Ferrotec Corp. (Taiwan). Diesel produced by the CPC Corp (Taiwan) is used as the miscible surrounding fluid. The specifications (with no external magnetic field) of both the magnetic fluid and the diesel are listed in Table I. Due to the magnetoviscous effect,[28] we also measure the initial viscosity of the EMG 905 when subjected to perpendicular external magnetic fields of various strengths, using a capillary tube viscometer with the same structure as that used by Li *et al.*[27] The corresponding initial magnetic susceptibilities of the fluids are listed in Table II, as calculated from the magnetization curve given by Ferrotec Corp. ($\chi = M/H$,

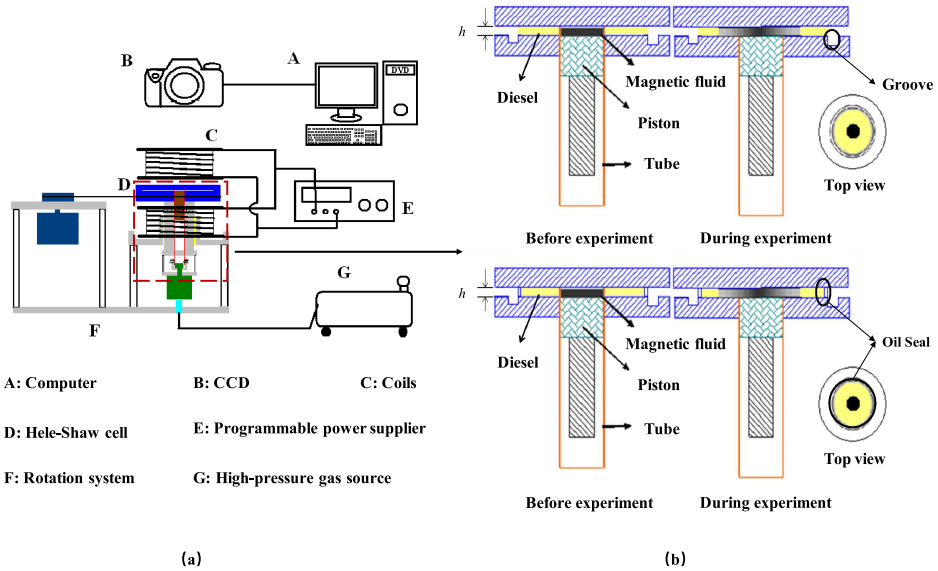

FIG. 1. (a) Sketch of the experimental apparatus, which consists of a rotating Hele-Shaw cell and a pair of Helmholtz coils, combined to produce a uniform, perpendicular magnetic field. (b) Blowups show the side views of the Hele-Shaw cell setup, with a miscible magnetic drop confined in a Hele-Shaw cell before the experiment (left) and an expanding miscible magnetic flow (right) during the experiment. The upper right and the bottom right figures represent the cases of open-flow and closed-flow conditions, respectively. Top views for both of these cases are shown. Magnetic fluids (black region) and their surrounding fluids (yellow region) are both confined in the Hele-Shaw cell. The tube, depicted by the orange line, works as a mobile divider to quarantine magnetic fluids and diesel, and this tube is retracted downward by a pneumatic piston controlled by the high-pressure gas source (G). The two miscible fluids are in contact thereafter.

where M stands for magnetization and H stands for magnetic field strength). We can see that the viscosity of the magnetic fluid increases with the increasing strength of the magnetic field, whereas the level of susceptibility shows the opposite trend.

The initial concentration gradient of the mixing interface is validated to reinforce the fingering instability.[7] Therefore, a jump in the concentration of fully magnetized ferrofluids is desirable for maximizing the concentration gradient during the initial mixing. To realize this jump in concentration, a mobile circular divider at the center of the Hele-Shaw cell (similar to the setup described in Ref. 15) is designed to seal the upper plate and to initially divide the regions for the magnetic fluids and the diesel. Magnetic fluids are injected into the inner region of the divider to form a drop with an initial radius of R_0. Then, the non-magnetic fluid (diesel) is injected into the outer region of the divider to become the surrounding fluid. This prevents premixing of the fluids before the experiment begins. The mobile divider is retreated downward for a height of the gap width precisely by a pneumatic piston (shown as the green part under the Hele-Shaw cell in Fig. 1), so that its top lies on the same plane of the bottom plate to start experiments. An oil seal is used to form a space h mm thick, confined between the two plates. This gap leaves an external boundary for the confined fluids in the Hele-Shaw cell to contact the atmosphere and form an open-flow Hele-Shaw cell. We also design a closed-flow Hele-Shaw cell to investigate the countering pressure gradient effect. The only difference between this and the open-flow case is that a circular sealed wall is set up during the closed-flow experiments. This wall forms a circle with a 60 mm radius right inside the circular groove, as shown in the bottom-right image in Fig. 1(b), making a concentric circle within the circular divider. Once the experiment begins, the interfacial morphologies of the magnetic drop are recorded and imaged by a charge-coupled device camera (Pulnix, TMC-7, 640 × 480 pixels), which allows the fingering instability to be analyzed. The moment when the mobile divider is retracted and the rotation begins is defined as the start time (t = 0 s) for each experiment. In experiments subjected to an external magnetic field, the magnetic drop is magnetized for 20 s in advance of the experiment's

TABLE II. Viscosity and susceptibility of EMG 905, as subjected to external perpendicular magnetic fields of different strengths.

Applied magnetic field H (Oe)	0	100	300	500
Susceptibility χ	3.47	1.70	0.87	0.13
Viscosity η (cP)	6.00	6.67	7.15	7.24

TABLE I. Specifications for the magnetic fluid, EMG 905, and diesel.

Fluid type	Saturation magnetization M_s (gauss)	Viscosity η@27°C (cP)	Avg. particle size (nm)	Initial susceptibility χ	Density ρ (g/ml)	Volume particle concentration (%)
EMG 905	440	6	10	3.47	1.20	7.8
Diesel	···	2.72	···	···	0.82	···

start time (when the divider is lowered and the rotation begins).

III. RESULTS AND DISCUSSION

A. Global flow image analysis

As the flow features for both the open-flow and the closed-flow cases are generally similar, we use the open-flow cases to depict the flow characteristics in Subsections III A 1 and III A 2. A comparison of the differences in flow features between the open-flow and closed-flow cases is given in Subsection III A 3. The effects of different gap depths on the flow features are presented in Subsection III A 4.

1. Rotational experiments without magnetic fields

The rotational experiments without a magnetic field for the open-flow case are shown and analyzed first. The images in Figs. 2(a)–2(c) show the magnetic drop of EMG 905 from the start (t = 0 s, as explained in Sec. II) to the end of the experiment (at which the Rayleigh-Taylor instabilities reach the boundary of the Hele-Shaw cell) at different rotational speeds, ω. The gap depth of the Hele-Shaw cell in these experiments is h = 1.00 mm, and the initial radius of the magnetic drop is 7.5 mm (R_0 = 7.5 mm). As shown in Figs. 2(a)–2(c), the density of the surrounding fluids (diesel) is lower than the density of the magnetic drop samples (as given in Table I). The fluids are thus displaced by the magnetic drop, so that the Rayleigh-Taylor instabilities occur on the interface between the fluids and the magnetic drop of EMG 905. A fairly uniform set of patterns is observed, consistent with the patterns obtained numerically by Chen.[22] Over time, tiny fingerings appear in the interfacial region between the miscible fluids. These fingerings grow slowly when the rotation speed is 100 rpm, but at a speed of 150 rpm the instabilities become more intense and the fingerings develop more quickly. Finally, at a speed of 200 rpm, the fingerings extend much faster and more dramatically, requiring only 20 s to expand out to the boundary of the Hele-Shaw cell. The fingerings appear in higher numbers at higher rotational speeds.

In the absence of a magnetic field, the growth of the magnetic drop is affected by two main factors: the diffusion between the two miscible fluids and the centrifugal force exerted by the rotation of Hele-Shaw cell. The rotational motion provides the centrifugal acceleration for the Rayleigh-Taylor instability that occurs between the magnetic fluids in the cell's center and the surrounding diesel, which have different densities. No obvious diffusion surrounding the tiny fingers is observed. Therefore, the rotation of the Hele-Shaw cell clearly plays a primary role in causing interfacial instability, and this density-related effect allows the centrifugal force to be maximized.[23] Similar to the effect of the gravitational field, it seems that the rotation of the Hele-Shaw cell provides a "centrifugal field" for the fluids within it, and the resulting convection is induced mainly by the centrifugal force. The small gap depth provides a force that is quite equivalent to the gravitational potential along the gravitational field in the z-direction. However, along the r-direction, the centrifugal force due to rotation offers a linear increase in the control volume along the radius outward from the axis of rotation. Therefore, the growth rate tends to be accelerated toward the edges of the cell due to the larger centrifugal force, and a similar effect on the density-driven Rayleigh-Taylor instability[29] can be identified. It is worth noting that the sharp (pointy) fingers observed in the current experiment in the absence of a magnetic field (Fig. 2) are not shown in the numerical simulations reported by Chen's group,[22,23] in which the tips of the fingers are more rounded. This difference could be caused by the three-dimensional effect. In these numerical simulations, two-dimensional analyses are performed with the implementation of Darcy's Law. However, the three-dimensional effect is inevitable in the experiment. According to light inspection tests, the miscible fluids appear nearly opaque for a concentration of magnetic fluids greater than 5%. As a result, the pointy fingers may represent the leading magnetic fluid streams inside the narrow gap caused by the rotation. Another possible reason may be the numerical diffusivity induced on the interface and the mesh resolution in the numerical resolution. Because Refs. 22 and 23 do not provide any experimental validation or grid independence tests, it is unclear whether the meshes used in the numerical simulations could resolve these initial fine-fingering phenomena. These sharp (pointy) fingers can only be resolved with a very high mesh resolution.

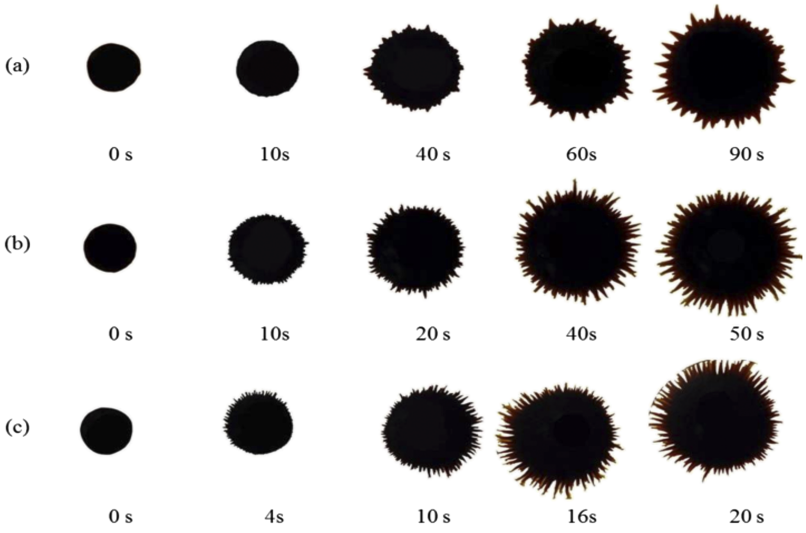

FIG. 2. Instability growth track of rotating magnetic drops without a magnetic field. Sections (a)–(c) show the growth of magnetic drops of EMG 905 at speeds of 100 rpm, 150 rpm, and 200 rpm, respectively.

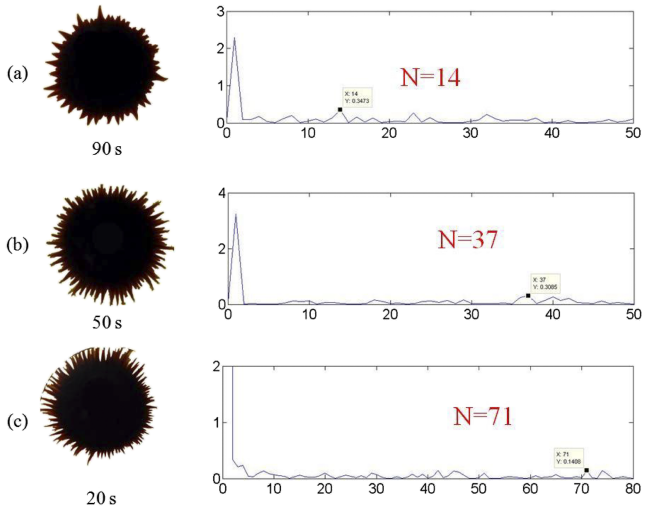

FIG. 3. Fast Fourier transformation (FFT) analysis of EMG 905 at the end of the experiments, for calculating the numbers of fingerings without a magnetic field at speeds of (a) 100 rpm, (b) 150 rpm, and (c) 200 rpm. N denotes the number of fingerings. The experimental images are shown on the left, and the corresponding FFT analyses are shown on the right.

To better evaluate the number of fingerings, we calculate the numbers from the polar representation of fingerings by defining the position of each point on the interface with its corresponding radius and polar angle.[15] A Matlab program is written to transform the color image file into an eight-bit gray-level bitmap file (with a gray-level value of 255 as pure white). The radius r of the mixing interface is found by taking the concentration contour with a specific gray-level value as a function of the polar angle. Fast Fourier transformation (FFT) is then applied to the polar representation (r, θ) of the fingering distribution along the interface. The number of Rayleigh-Taylor fingerings that characterizes the instability is found in the second largest peak in the power spectrum amplitude, as shown in Fig. 3. We find that 71 thin fingerings are induced at a speed of 200 rpm but only 37 at 150 rpm and 14 at 100 rpm. These numbers of fingers represent the fastest growing Fourier modes. Therefore, a higher rotation speed produces larger numbers of thinner fingerings. These experimental results are consistent with Chen's predictions[22] made by numerical simulations of miscible fluids in a rotating Hele-Shaw cell. Both of these experiments demonstrate that a higher rotation speed enhances instability, causing larger numbers of fingerings.

2. Experiments with magnetic fields

Typical images of the experimental results with a magnetic field for the open-flow cases are presented in Figs. 4–6. The magnetic drop is fully magnetized before the divider is removed and the rotation begins at $t = 0$ s. Triggered by the presence of a magnetic field, the secondary waves are formed initially, as Wen *et al.*[15] observed in the interfacial region and further validated analytically in Section III B 3 below. When the Hele-Shaw cell is motionless under the action of a perpendicular field, as in the work of Wen *et al.*,[15] at the later stage of the experiment, the interfacial region of the miscible drop evolves into a number of secondary waves resembling round *Prunus mume* petals. With the rotation motion of the Hele-Shaw cell, the incipient secondary waves elongate to form a unique swinging instability pattern, with the so-called main fingerings indicated by the arrows in Fig. 4. These secondary waves become elongated instantly because of their large mass in comparison with the tiny fingers by the centrifugal force and are more elongated by the rotation motion than in the case without a magnetic field. Generally, the petal size of the secondary wave is not truly uniform. Therefore, the secondary waves with larger petals will be elongated more than the smaller ones, yielding the different length of each main fingering.

It is noteworthy that before the divider is lowered, the magnetic fluid is fully magnetized under a non-rotation condition. Once the divider is removed, the labyrinthine fingerings emerge immediately. Rotation begins once the divider is removed, and as the secondary waves form, they are instantly exposed to the rotation flow as well. These effects combine to cause a more rapid break-out from the quasi-stationary state than is seen with vigorous rotation alone. The secondary waves are elongated outward, leading to the prominent development of main fingerings. These developments are shown in Figs. 4–6, specifically for the early period of $t \leq 20$ s.

The instabilities of EMG 905 are observed at a constant magnetic field strength, but with various rotation speeds. Figs. 5(a)–5(c) show that more intensive instabilities occur (with

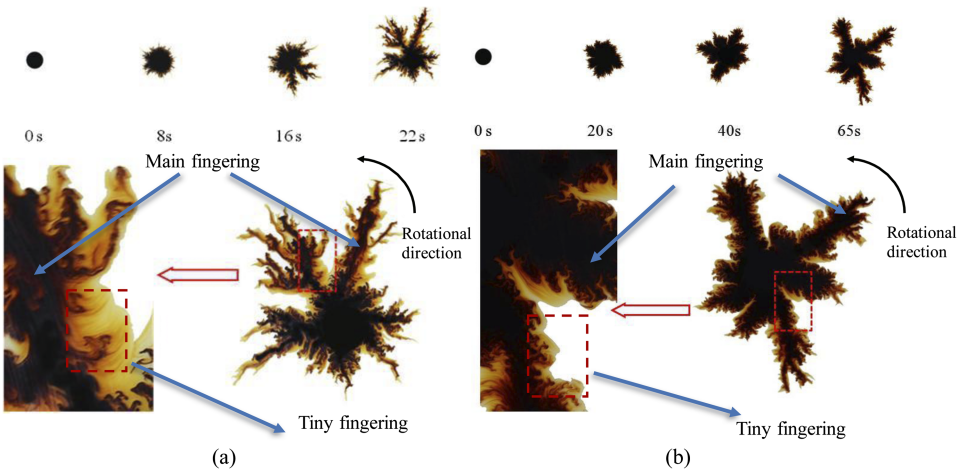

FIG. 4. Instabilities of EMG 905 subjected to $H = 300$ Oe and $\omega = 200$ rpm. (a) A case involving open flow is shown, with a section of the image at $t = 22$ s magnified on the lower left side. (b) A case with closed flow is shown, with a region of the image at $t = 65$ s magnified on the lower left side. The difference between the main and tiny fingerings is identified by blue arrows. The rotational direction is counterclockwise, as denoted by the black arrows.

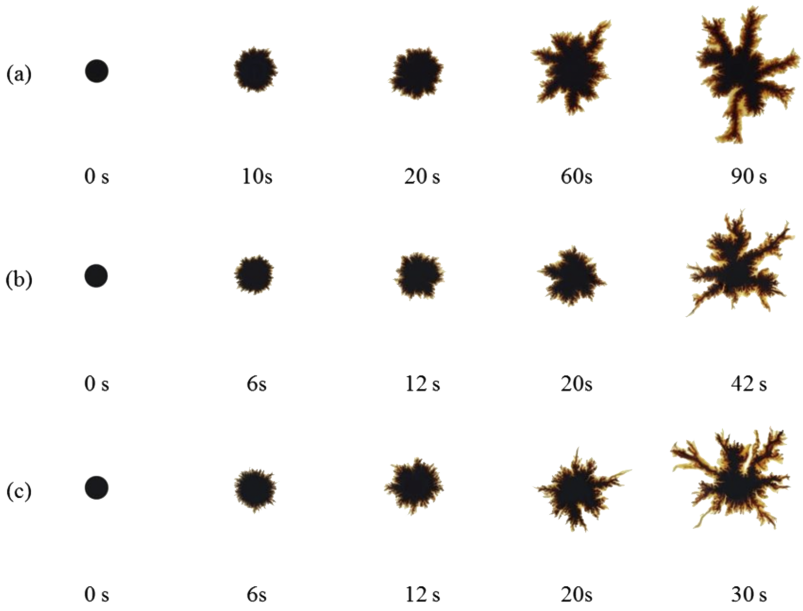

FIG. 5. Instabilities of EMG 905 in an open-flow rotating Hele-Shaw cell, confined in a gap with a depth of $h = 1.00$ mm and subjected to a magnetic field of $H = 500$ Oe at several rotation speeds: (a) $\omega = 100$ rpm; (b) $\omega = 150$ rpm; (c) $\omega = 200$ rpm.

sharper tiny fingerings and larger areas covered by the magnetic drops) at higher rotation speeds (e.g., see the comparison at $t = 20$ s). As the magnetic drop is subjected to a stronger centrifugal force pushing it outwards, it takes less time to expand. The rotation effect is also similar to that seen under the condition without a magnetic field.

By comparing the results shown in Figs. 6(a)–6(c) at the same rotation speed of 100 rpm, it can be seen that a stronger magnetic field leads to more intensive instabilities with increasing numbers of tiny fingers, and a larger area of the magnetic drop at the same point in time ($t = 20$ s). Labyrinthine instabilities occur mainly because the magnetic nanoparticles within the magnetic fluids always align with the perpendicular magnetic field, and their dipolar forces keep repulsing each other.[15] This is how a stronger magnetic field helps to induce more intensive tiny labyrinthine instabilities and more growth in the main fingerings. Nevertheless, due to the lack of constraint of the surface tension, mass diffusion must come into play along with the rotation motion. The vigorousness of the labyrinthine fingers induced in the early stage is weakened by the natural diffusive mixing. The local concentration of the magnetic fluids decays continuously and can be identified by the lighter colored zone adjacent to individual fingers, as seen in the images taken later in the experiment in Fig. 6. When the strength of the magnetic field increases, the number of labyrinthine fingers increases and the interfacial length increases accordingly. The magnetic fluids have a longer contact length to diffuse into the surrounding miscible fluids on the later evolution of the ensuing instabilities, leading to stronger dispersive effects. Therefore, an area of much lighter color is shown in the interfacial region in Fig. 6(c) than Fig. 6(a). The lighter area adjacent to the main fingerings can also be clearly observed in Figs. 4 and 5. The miscible interface is stabilized by the mass diffusion.

Another observation of interest is that the main fingerings shown in Figs. 6(a)–6(c) extend to the boundaries of

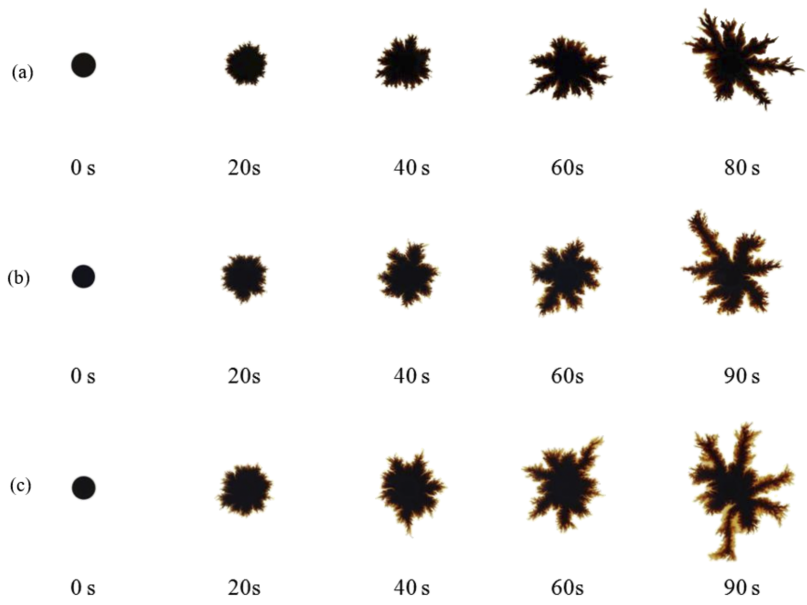

FIG. 6. Instabilities of EMG 905 in an open-flow rotating Hele-Shaw cell with a gap depth of $h = 1.00$ mm, at the rotation speed of $\omega = 100$ rpm, subjected to various magnetic fields: (a) $H = 100$ Oe; (b) $H = 300$ Oe; (c) $H = 500$ Oe.

the Hele-Shaw cells at similar speeds (t = 80 s, 90 s, and 90 s, respectively) when subjected to magnetic field strengths of H = 100 Oe, 300 Oe, and 500 Oe. With magnetic field strengths of H = 300 Oe and H = 500 Oe, the magnetic drops show similar rates of growth, with ending times at 90 s. At H = 100 Oe, the shorter ending time of 80 s represents a faster growth rate. These results show that a weaker magnetic field helps the fingerings to reach the cell's fringe earlier. However, as we mentioned previously, at t = 20 s a more intensive expansion of magnetic drops under stronger magnetic fields has been validated. This paradox seems to show that the magnetic field has opposite effects at different stages, but actually the results just show a reduction in the rate of acceleration, with greater facilitation of drop growth in the early period and reduced facilitation in the later period. For the early period, a stronger magnetic field yields a more viscous magnetic fluid, and the contrast in viscosity with that of the surrounding diesel is enhanced, as indicated in Table II. Magnetic fluid with increased viscosity has a larger friction drag. However, a stronger magnetic field also enhances the magnetic dipolar repulsion, so that the opposing effects are both amplified under an increasingly strong magnetic field, and the net outward-growth tendencies appear at similar stages.

3. Comparison of the flow features between the open-flow and closed-flow cases

In the open-flow cases, the magnetic drop shows a significant tendency to expand as time elapses, which is attributable to two effects: the repulsion interaction between magnetic dipoles along the direction of the magnetic field, and more vitally, the rotation effect on the magnetic fluids in the open-flow case. The results are similar for the closed-flow cases, so we only show representative results for the comparison between open-flow and closed-flow cases. Comparing Fig. 4(a) for the open-flow and Fig. 4(b) for the closed-flow cases (which are both measured under the same magnetic field of 300 Oe and at the same speed of 200 rpm), a countering pressure gradient effect induced by the closed-flow design is apparent. As in the case given in Ref. 23, the characteristic pressure can be expressed by $\Delta\rho\omega^2{R_0}^2$, where $\Delta\rho$ is the density difference between the magnetic fluid and the surrounding diesel, so that the pressure gradient can be derived by $\Delta\rho\omega^2{R_0}^2/R_0 = \Delta\rho\omega^2R_0$. This pattern is similar to the form of the characteristic centrifugal force, $\rho\omega^2R_0$. Physically, the countering pressure gradient is caused by the rotation of the Hele-Shaw cell and the constraint of the outer wall. These conditions stop the flow from being pushed further outward, which causes them to generate a countering pressure gradient opposite to that of the centrifugal force; hence, both cases share similar formulas. Therefore, alongside the driving effect of the centrifugal force, the countering pressure gradient provides a resistive effect to stabilize the growth of labyrinthine instabilities. This effect lengthens the growth time of the magnetic drop from 22 s (as shown in Fig. 4(a)) to 65 s (as shown in Fig. 4(b)). The main fingerings appear at t = 16 s without a countering pressure gradient, and at t – 40 s with a countering pressure gradient. This delay is obviously an effect of the countering pressure gradient. Compared with the intensive trend seen in Fig. 4(a), both the main fingerings and the tiny fingerings around them tend to extend in a much slower, milder, and blunter way. This pattern indicates that the countering pressure gradient actually calms and stabilizes the instabilities, which consequently become wider. The miscible mixture process also becomes slower, as shown by the heavier color on the interface. Therefore, the countering pressure gradient triggers a relatively smooth interfacial region.

The tiny labyrinthine fingerings bend in a counterclockwise direction, the same as the rotational direction, which is consistent with predictions based on the theoretical model derived by Waters and Cummings.[18] These results confirm the existence of labyrinthine fingerings that lag behind the main fingerings. This development is attributable to the Coriolis effect, which appears due to the rotating motion of the Hele-Shaw cell. In addition, these tiny labyrinthine fingerings tend to mix with the diesel and fade away off the main fingerings, due to a decrease in the concentration as indicated by a lighter color around the interface region. It should be noted that a dimensionless parameter, Rossby number Ro, can be defined by the ratio of the characteristic Coriolis force to the characteristic centrifugal force, where ωR_0 is used for the tangential velocity scale, which exactly follows the form of Eq. (24) in Emslie *et al.*:[20]

$$Ro \equiv \frac{\rho_0 R_0 \omega^2}{2\rho_0 \omega(\omega R_0)} \sim 0.5. \tag{1}$$

Emslie reported that the condition for neglecting the Coriolis effect is that this ratio, Ro, should be much smaller than 1. In our case, however, the magnitude of Ro is approximately equal to 0.5, which indicates that the Coriolis force and the centrifugal force are similar in scale. This finding indicates the significance of the Coriolis effect in the whole rotating Hele-Shaw cell system. Therefore, the appearance of these distinctive tiny bending fingerings is validated, and is consistent with the significance of the Coriolis effect.

4. Hele-Shaw cell gap depth effect

The three-dimensional effect achieved by changing the gap depth from h = 1.00 mm to h = 1.30 mm is emphasized in Fig. 7. This figure illustrates a magnetic drop of EMG 905 when subjected to a magnetic field of H = 500 Oe, at the speed of ω = 100 rpm. Comparing Figs. 7(a) and 7(b) at the same elapsed time of t = 40 s, we see that a magnetic drop confined in a gap with a depth of h = 1.3 mm shows more aggressive growth than the drop set in a shallower gap. The ending time of 55 s in the case with h = 1.3 mm is also much earlier than the 90 s ending time for the case with h = 1.00 mm. In the larger gap, the chain of magnetic nanoparticles along the magnetic field is more elongated than in the case with a shallower gap. This elongation reinforces the repulsion among all of the chains, due to the stronger summing of magnetic dipoles from more magnetic nanoparticles, and hence the magnetic effect is more prominent. As the viscous force in this system is generally expressed by $12\eta u/h^2$, where u is the velocity, the viscous force can also be reduced in a quadratic way by a greater gap depth h. With the help of this reduction of viscous force, the magnetic fluid is able to expand outward in a much easier and faster way, and thus the time needed for maximal growth is reduced from 90 s for h = 1.00 mm to 55 s for h = 1.30 mm.

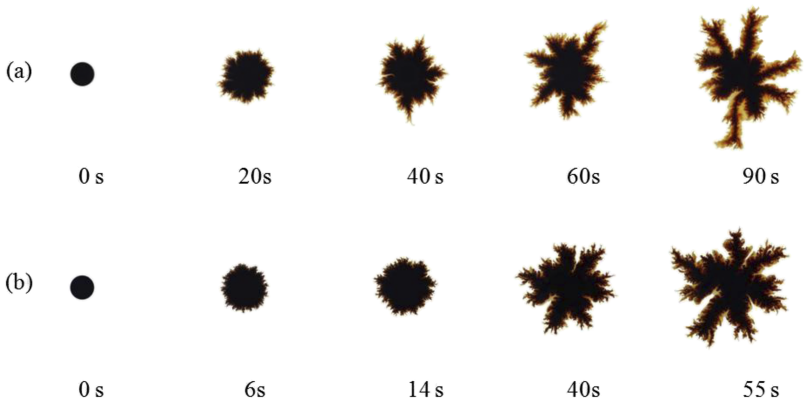

FIG. 7. Instabilities of magnetic fluid (EMG 905) samples in an open-flow Hele-Shaw cell under the experimental settings of H = 500 Oe and ω = 100 rpm, but with different gap depths of (a) h = 1.00 mm and (b) h = 1.30 mm.

Another extraordinary feature is the darker color that appears in the interfacial region when h = 1.30 mm. For example, at t = 40 s in the case of h = 1.3 mm, the darker color indicates that the diffusion and mixing process in the interfacial region is slower. As mentioned before, the larger gap accelerates the expansion of the magnetic drop, and the advection is therefore greatly enhanced. As a result, a larger gap reduces the time required for the diffusion mixing process. Another interesting observation is that comparing the incipient secondary waves at t = 20 s in Fig. 7(a) and at t = 14 s in Fig. 7(b), a more uniform petal size (wavelength) of the secondary wave is observed for h = 1.30 mm. This observation is consistent with that in Kao's thesis.[30] When the gap depth h increases, the magnetic Péclect numbers (the ratio of the characteristic magnetic advection rate and the diffusion rate, as introduced in Eq. (4) in Sec. III B) increases accordingly. The instabilities of a miscible magnetic fluid drop in a Hele-Shaw cell will further develop into the three-dimensional Stokes regimes presented by Fernandez,[29] yielding a more uniform petal size (wavelength) of the secondary wave. As mentioned, the length of the main fingering is sensitive to the initial petal size due to the rotation effect; thus, when h = 1.30 mm, the main fingerings are of similar lengths.

B. Interfacial instability analysis

1. Dimensional parameters

To better characterize the instabilities in this rotating Hele-Shaw cell system with an external perpendicular magnetic field, it is necessary to establish the relevant dimensional parameters associated with the magnetic field and the rotation. Based on the experimental observations described above, the advection in this system clearly arises from two major factors: the interaction between the magnetic fluid and the magnetic field, and the centrifugal force due to rotational motion. However, both of these forces are moving in the opposite direction to the viscous force, with a scale of $12\eta u/h^2$. The scale of the magnetic force is $\mu_0\chi H^2/R_0$, and that of the centrifugal force is $\rho_0\omega^2 R_0$. The notations included in these formulas are η for the initial viscosity of magnetic fluid, u for the velocity scale, μ_0 for the magnetic permeability in free space, χ for the initial susceptibility of magnetic fluid, H for the external magnetic field strength, ρ_0 for the initial density of the magnetic fluid, and ω for the angular speed of the Hele-Shaw cell. Two length scales are involved: R_0, which is the initial radius of the magnetic drop for the length scale on the cell's plane, and h, which is the gap depth of the Hele-Shaw cell, and acts as the length scale on the perpendicular direction of the cell. Therefore, two velocity scales are introduced for characterizing the corresponding magnetic and rotational effects:

$$\mathrm{U}_m = \frac{\mu_0\chi H^2/R_0}{12\eta/h^2} = \frac{\mu_0\chi(Hh)^2}{12\eta R_0}, \tag{2}$$

$$\mathrm{U}_c = \frac{\rho_0\omega^2 R_0}{12\eta/h^2} = \frac{\rho_0(\omega h)^2 R_0}{12\eta}. \tag{3}$$

Two modified Péclect numbers are obtained, based on these two velocity scales:

$$\mathrm{Pe_m} \equiv \frac{\mathrm{U}_m R_0}{D} = \frac{\mu_0\chi(Hh)^2}{12\eta D}, \tag{4}$$

$$\mathrm{Pe}_c \equiv \frac{\mathrm{U}_c R_0}{D} = \frac{\rho_0(\omega R_0 h)^2}{12\eta D}. \tag{5}$$

The initial radius is regarded as the length scale for the Péclect numbers (namely, Pe_m for the modified magnetic Péclect number, and Pe_c for the modified rotation Péclect number). This scale is adopted because the evolution of the magnetic drop within the Hele-Shaw cell is observed from the top; therefore the measurements are mainly focused on changes in the radial and azimuthal directions. Furthermore, the contribution from the diffusion rate along the radial direction can be compared to the contributions from the magnetic field or the rotation motion, and these two modified Péclect numbers are used for analysis on the instabilities in the following analyses.

2. Magnetic effect and rotation effect

To quantify the displacement of the instabilities, Matlab software is used to read and analyze the scanned experimental images. This analysis allows us to calculate the radius and radian for each point on the mixing interface of the magnetic drop for each experimental image. The radius of gyration, R_g, is obtained by averaging all of the radii of points at the interface from the center, and the interfacial length L is obtained by adding the distance between all pairs of neighboring points. Furthermore, the dimensionless radius of gyration, R_g*, is obtained. The radius of gyration scaled by the initial radius of the magnetic drop (at t = 0 s) and the dimensionless length of the mixing interface L* are similarly obtained and used as

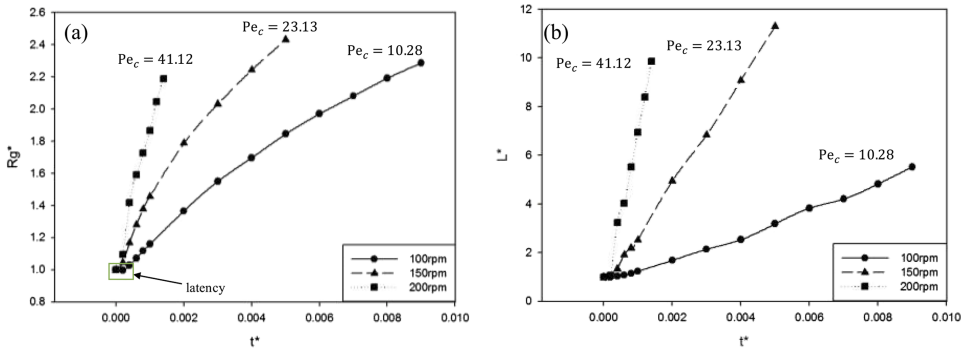

FIG. 8. Growth curves of EMG 905, with different rotation speeds and corresponding values of Pe_c: (a) the growth of a dimensionless radius of gyration, and (b) the growth of a dimensionless length of the mixing interface. No magnetic field is imposed.

measures to quantify the drop growth. The time t is scaled by $2\pi/\omega$.

For the case without an external magnetic field, Fig. 8 shows that both R_g* and L* increase with time, and they grow faster at higher rotational speeds. This growth can be divided into two stages: a short period of latency, and a period of linear growth toward the asymptotic maximum. Mathematically, the concave shape of the growth rate indicates the second order derivative of gyration with respect to time, such that the growth rate decreases with time. This result implies that the acceleration of the magnetic drop's physical expansion is reduced in conditions where only rotation is imposed. As the centrifugal force is proportional to the distance from the rotation center and to the density at a given rotation speed, measures for the prevention of growth can be concentrated on varying the density and viscosity of the fluids due to their miscibility, especially for the interfacial region. During the expansion process, the mixing activity thus happens on the interface. This activity makes the gradients of density and viscosity on the interface milder, which weakens the intensity of the instabilities.

The numerical experiments conducted by Chen and Wang[22] indicated that a heavier and more viscous fluid droplet, when surrounded by miscible fluid with a lower density and viscosity, provides a more aggressive outward driving force. Our experiment also shows that decreasing the density and viscosity of the droplet leads to weakening of acceleration as the mixing process proceeds. As for the immiscible case, Carrillo[24] experimentally discovered a short latency period and sequential exponential growth, followed by consistent linear growth. This pioneering experiment showed a continuous trend with no weakening of acceleration, because the immiscible fluids did not come to realization in the mixing process and their density and viscosity could remain in their original state throughout the process. Nevertheless, the latency period of gyration is successfully observed for the miscible case in our experiments, as indicated by the arrows in Fig. 8, and this finding is consistent with the simulations conducted by Chen[22] and the experiments performed by Carrillo.[24]

When affected by the rotational motion of the Hele-Shaw cell system, the growth of a magnetic drop branches out from the latency period into three different growth curves with different Pe_c values, even though the overall tendencies are similar. The curve of Pe_c = 10.28 (ω = 100 rpm) shows a relatively mild growth trend, which takes twice as long to reach a given gyration radius than the curve of Pe_c = 23.13 (ω = 150 rpm). The curve of Pe_c = 41.12 (ω = 200 rpm) shows a much steeper growth trend, which is consistent with the results of global flow analysis for the non-magnetic case described in Sec. III A 1. A higher Pe_c value leads to faster growth of the magnetic drop, because the faster rotational motion can easily induce strong advection of the fluids by pushing them outward, and the EMG 905 fluid, being heavier than diesel, can be driven by centrifugal force to expand further.

To capture the effect of the magnetic field, the growth curves of cases with an imposed magnetic field are presented in Fig. 9. These curves show that for cases subjected to magnetic fields of the same strength but at different rotational speeds, the magnetic drops grow at similar rates, and thus the gyration

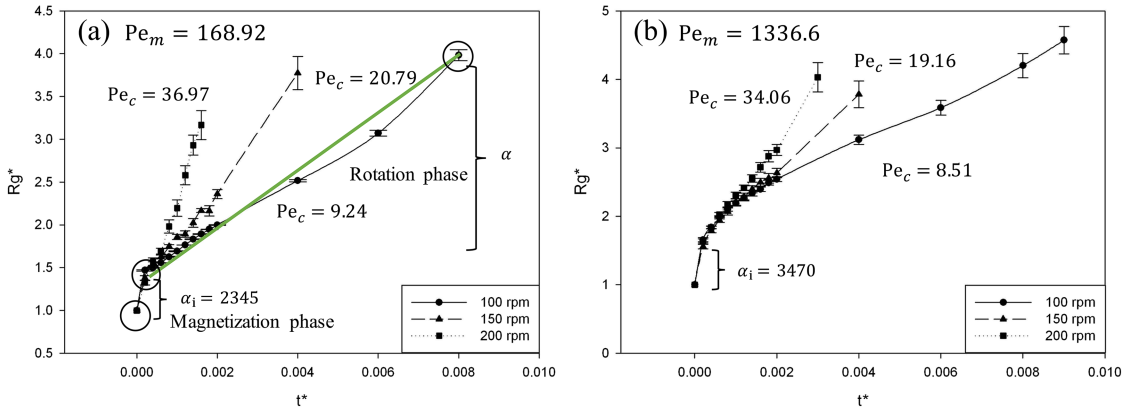

FIG. 9. Growth curves for the open-flow case, with a corresponding initial growth rate α_i. The results for EMG 905 are (a) Pe_m = 168.9 (H = 100 Oe) and (b) Pe_m = 1336.6 (H = 500 Oe). The values of Pe_c for different speeds and magnetic fields are also listed beside the curves. In (a), two phases of magnetic drop growth are emphasized: a magnetization phase with initial growth rate α_i, and a rotation phase with rotation growth rate α.

radii at the three different speeds are almost the same at the preliminary stage, especially for the first two measured moments. Unlike the cases without a magnetic field, no latency period is observed. Instead, the extraordinarily steep growth at the preliminary stage reflects a strong tendency for exponential growth. The initial growth rates at the preliminary stage, as defined by $\alpha_i = dR_g^*/dt^*$ for the first two moments, are shown for each case in Fig. 9(a). For EMG 905, an α_i subjected to a stronger magnetic field is higher than that in a weaker field, as seen by comparing Figs. 9(a) and 9(b). Therefore, the α_i seems to be highly magnetic-field-dependent. The reason for this effect is that the magnetization of the magnetic drop before the start of the experiment makes the magnetic nanoparticles within the magnetic fluids align along the direction of the magnetic field, which leads to an intensive dipolar repulsion interaction before the divider is lowered. Once the divider has been lowered, this intensive interaction pushes the magnetic drop so that instabilities develop outward. The pattern whereby a stronger magnetic field leads to more intensive dipolar repulsion is indicated by Eq. (4). As the $\mathrm{Pe_m}$ is larger, the same sample subjected to a stronger magnetic field has a faster rate of growth, and therefore the advection induced by the magnetic field becomes more rigorous. In addition, the rotation begins at the moment the divider is lowered, and then takes 1–3 s to reach the setting speed, so that the rotation effect is smaller than the magnetic effect at first, and the initial growth of the magnetic drop is dominated by the magnetic effect. We therefore define this stage as the "magnetization phase" due to the significance of the magnetic effect, as illustrated in Fig. 9(a).

Focusing on the difference between the growth trends with and without a magnetic field, we see that the magnetic field triggers the emergence of repulsions between the magnetic dipoles, which contribute to the sequential facilitation of growth following the magnetization phase. This growth facilitation can be observed by comparing Figs. 8(a) and 9(a), where the value of Pe_m is 0 (without a magnetic field, H = 0 Oe) and 168.92 (with a magnetic field, H = 100 Oe), respectively. The advection of magnetic fluid from the center is facilitated by the magnetic effect, as shown by the increasing Pe_m. At t^* = 0.002, as shown in Fig. 8(a), the ($\mathrm{Pe_m}$ = 0) $R_g{}^*$ values are about 1.4, 1.7, and 2.2 at rotation speeds of 100, 150, and 200 rpm, respectively, and the (Pe_m = 168.9) $R_g{}^*$ values are about 2.0, 2.2, and 3.5 in the corresponding cases in Fig. 9(a). It should be taken as confirmed that this growth facilitation results from the presence of magnetic fields. Nevertheless, in Fig. 9(b) the (Pe_m = 1336.6) $R_g{}^*$ branches are identified as around 2.5 for three rotation speeds, with longer periods for the overlaps among the curves, which have smoother turning points after the magnetization phase.

These interesting phenomena imply that when subjected to stronger magnetic fields, the magnetic drops can continuously retain strong magnetic dipolar repulsion even after their magnetization. Notably, the growth of the magnetic drops is strongly affected, as Pe_m is proportional to the square of the magnetic field strength, H. Therefore, the magnetic effect retains its significant effect on growth immediately after the magnetization phase. Then, as the magnetic drop keeps expanding, which weakens the magnetic dipolar repulsion, the effect of rotation emerges as the primary influence on drop growth. Another interesting feature is that for cases rotating at the same speed, the growth trends after the magnetization phase develop in similar ways, and begin to differentiate only in later periods even if they are subjected to magnetic fields of different strengths, as shown in Fig. 10. The Pe_c values are 9.2, 8.6, and 8.5 for cases with the same rotation speed of 100 rpm, but with different magnetic fields of 100, 300, and 500 Oe. This pattern arises because of the magnetoviscous effect, which varies the Pe_c value even for cases rotating at the same speed. However, compared with the much larger differences in Pe_m (168.9 for 100 Oe, 723.9 for 300 Oe, and 1336.6 for 500 Oe), the differences in $\mathrm{Pe_c}$ are relatively small, and the nuances of the rotation effect can therefore be considered negligible. The curves of $\mathrm{Pe_m}$ = 723.9 and $\mathrm{Pe_m}$ = 1336.6 are basically overlapping even after the "magnetization phase," and the difference evolves later, when the curve of $\mathrm{Pe_m}$ = 1336.6 is lower than that of $\mathrm{Pe_m}$ = 723.9. Although the magnetic dipolar repulsion is strengthened by a higher magnetic field, its opposite competitor, the viscous force, is also reinforced by the magnetoviscous effect, as indicated in Table II. Before the drops branch out, the net forces exerted on them are almost the same, but as time proceeds, their gyration radii continue to increase along with the reduction in the strength of dipolar repulsion. Therefore, the curve of $\mathrm{Pe_m}$ = 723.9, which has inherently lower viscosity, shows a higher growth rate after the branch than that of $\mathrm{Pe_m}$ = 1336.6, with its higher viscosity. Notably, in the case of $\mathrm{Pe_m}$ = 168.9, the weaker magnetization fails to generate and maintain sufficiently strong magnetic dipolar repulsions, so that the growth rate drops suddenly immediately after the magnetization phase, and the growth curve for this case is much lower than that of the other two cases.

As for the rotation effect, once the rotation stabilizes at the setting speed, the rotating flow in the Hele-Shaw cell is driven by centrifugal force, which pushes the gyration radius to increase rapidly. By definition, Pe_c supports the prediction that for the same sample and the same magnetic field strength, the advection induced by rotational motion can be strengthened

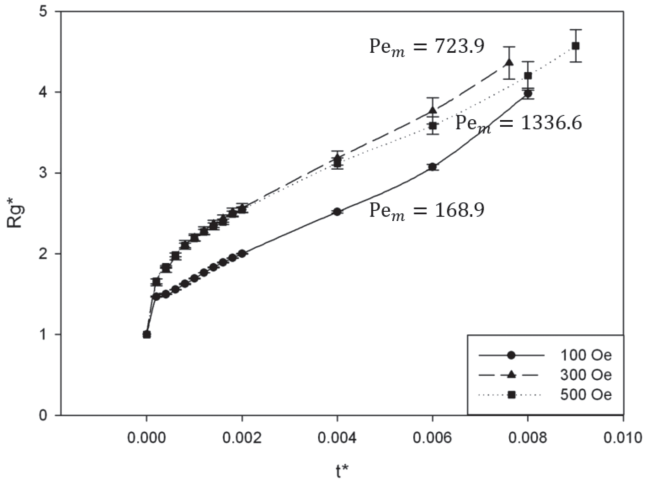

FIG. 10. Growth curves for the open-flow case at a rotation speed of 100 rpm for EMG 905, subjected to different magnetic fields with different values of Pe_m and Pe_c: $\mathrm{Pe}_m/\mathrm{Pe}_c$ = 168.9/9.2 for 100 Oe, Pe_m/Pe_c = 723.9/8.6 for 300 Oe, and $\mathrm{Pe}_m/\mathrm{Pe}_c$ = 1336.6/8.5 for 500 Oe. (The values of Pe_c are not marked on the curves.)

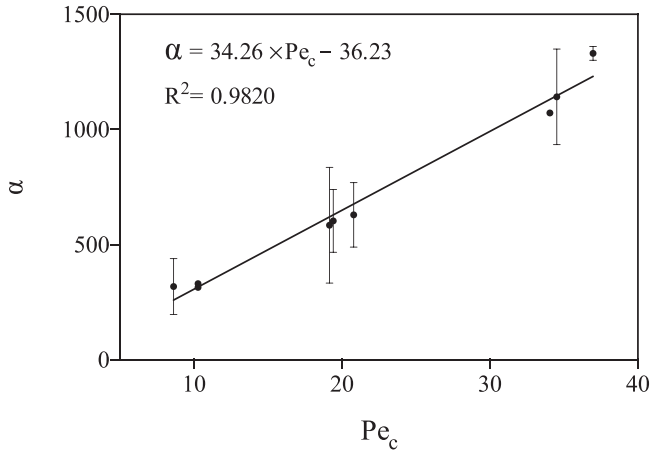

FIG. 11. Relationship between growth rate and modified Péclect number in the rotation phase for the open-flow case, with linear regression results.

with increasing rotation speed. In the later period, as shown in Fig. 9, the different growth rates in each case are directly related to the different rotational speeds, and higher speeds lead to quicker increases of gyration under the same magnetic field. This pattern is similar to that observed previously in cases without a magnetic field and with inherently different Pe_c values. Steeper curves can be clearly identified by higher Pe_c values, which indicate stronger advection by rotation. We denote this stage of the droplet's growth as the "rotation phase," as illustrated in Fig. 9(a), where the growth rate under rotation, α, is defined by the slope, $\alpha = dR_g^*/dt^*$, between the end time step of the magnetization phase and the end of the rotation phase. If we consider the tendency in the rotation phase, it appears obvious that α should be smaller than α_i, because the magnetization phase shows a steeper growth rate. This case provides a comparison to demonstrate that the magnetic effect due to dipolar repulsion is stronger than the rotation effect if the magnetic drop is held within a small area. In addition, the magnetic effect becomes weaker as the dipoles get further apart during the growth process, and the rotation effect then becomes dominant.

To further demonstrate the dominance of the rotation effect in the rotation phase, a linear regression between the rotation growth rate α and modified rotation Péclect number Pe_c is performed, as shown in Fig. 11. Good linear regression results are obtained with the regression parameter $R^2 = 0.9820$, which shows the significance of the rotation effect in the rotation phase, and verifies the feasibility of predicting the growth rate α based on the modified rotation Péclect number Pe_c. This case also shows that the growth rate α increases linearly with the rotation Péclect number Pe_c, according to the fitting equation $\alpha = 34.26Pe_c - 36.23$. It should be noted that the definition of Pe_c from Eq. (5) couples the rotation and the magnetoviscous effect due to the magnetic-dependent viscosity, as this combination of factors allows us to fully and precisely describe the effect of the magnetic field during the rotation phase.

In summary, during the "magnetization phase," the magnetic effect dominates the growth of instabilities, and thus the growth curves almost overlap for the cases with three differing rotation speeds, as the dipoles of the magnetic chains intensively repulse each other due to the small distances between them. However, in the subsequent "rotation phase," the rotation effect dominates the rate of growth. A higher rotation speed contributes to a faster growth rate, which linearly increases with the modified rotation Péclect number, Pe_c. Although the magnetic effect dominates and facilitates instabilities at the beginning, weaker growth is also induced by the magnetic influence due to the magnetoviscous effect, which acts as a non-monotonic influence on the instabilities.

3. Countering the pressure gradient and gap depth h effect

As discussed in Subsection III A, a countering pressure gradient suppresses the growth of the magnetic drop. The growth curves for the open-flow and closed-flow cases under the same experimental conditions are presented in Fig. 12. For the cases with $h = 1.30$ mm (shown in Fig. 12(a)) under the same Pe_c and Pe_m, the curve for the open-flow case shows steeper growth than that of the closed-flow case. This observation indicates that the growth rate in the open-flow situation is faster, and the closed-flow design suppresses the expansion of the magnetic drop due to the induction of a countering pressure gradient. Similarly, even when subjected to a stronger magnetic field, as shown in Figs. 12(b) and 12(c), the curves of the closed-flow case are still lower than those for the open-flow case under the same Pe_c and Pe_m. Unlike the coupled effect of the magnetic field, the countering pressure gradient provides a monotonic suppression effect on the instabilities.

In examining the definitions of Pe_c and Pe_m, we can see that both of these factors are proportional to h^2 (which originates from the viscous force term). Therefore, enlarging

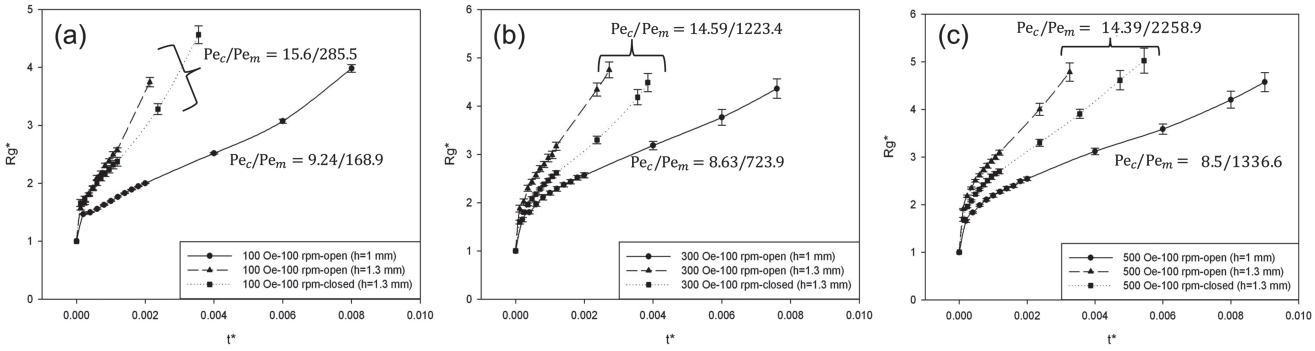

FIG. 12. Growth curves for EMG 905 at a rotation speed of 100 rpm, showing the effects of gap depth h (or of countering pressure gradients) subjected to different magnetic field strengths with the values of Pe_c and Pe_m embedded as follows: (a) $H = 100$ Oe, (b) $H = 300$ Oe, (c) $H = 500$ Oe.

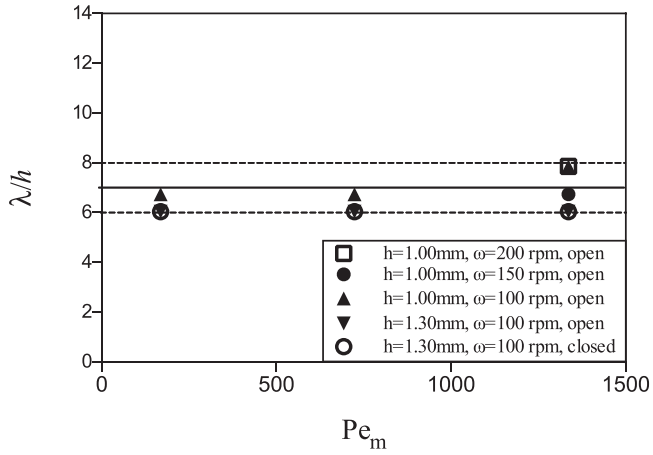

FIG. 13. Ratio of the wavelength λ and the gap depth h under different experimental conditions. The observed pattern closely follows the formula $\lambda/h \approx (7 \pm 1)$, with appropriate modification of the magnetic Péclect number.

the gap depth in the Hele-Shaw cell should clearly facilitate advection induced by either the centrifugal force or the magnetic field, due to the inversely quadratic reduction of viscous force. Accordingly, Fig. 12 shows that for open-flow situations like that illustrated in (a), the growth trends of cases with higher Pe_c and Pe_m (15.6 and 285.5, respectively) are much steeper than those with lower Pe_c and Pe_m (9.24 and 168.9, respectively), especially in the rotation phase. Similar patterns can be identified in Figs. 12(b) and 12(c). Nevertheless, it is of interest that the curves of all closed-flow cases with h = 1.30 mm are ahead of all curves for open-flow cases with h = 1.00 mm, even though the countering pressure gradient tends to suppress the instabilities. In terms of the Péclect numbers, closed-flow cases with h = 1.30 mm obtain higher values for both Pe_c and Pe_m, so that this increment in the gap depth clearly facilitates growth, and remarkably, can even overcome the barrier of the countering pressure gradient. In addition, variations in the magnetization phase clearly facilitate steeper growth at the first time step. This effect may be attributable to the increase of Pe_m, based on the increment of h as discussed in Sec. III A 4.

As Wen[15] reported, when subjected to a steady, normal external magnetic field, secondary waves are formed on the miscible interface, and the corresponding wavelength λ is determined by $\lambda = 2\pi R_0/n$, where n represents the number of secondary waves. The correlation between the wavelength λ and the gap depth h follows the formula $\lambda \approx (7 \pm 1)\,h$. The relationship illustrated in Fig. 13 can be obtained by calculating λ and treating n as the number of main fingerings. The ratio of wavelength and gap depth, λ/h, lies in the range of 7 ± 1, even if the value of Pe_m keeps increasing. This pattern is similar to that of the Stokes regimes of Rayleigh-Taylor instabilities presented by Fernandez,[29] which shows a constant ratio of wavelength to gap depth when the Péclect number is sufficiently large. Based on this consistent pattern, we conclude that the main fingerings growing in a rotating Hele-Shaw cell are developed by secondary waves. In the magnetization phase, secondary waves are formed and elongated by centrifugal force, due to the rotational motion of the Hele-Shaw cell. This process results in the formation of the main fingerings, as shown in Fig. 4.

IV. CONCLUSION

This study experimentally and systematically analyzes the instabilities and growth of magnetic fluids with miscible diesel confined within a rotating Hele-Shaw cell. Major effects are measured and compared in a series of experiments using magnetic fluid samples (of EMG 905), and the relevant parameters (Pe_c and Pe_m) are derived to evaluate the instabilities and growth of magnetic drops.

Unlike the sharp labyrinthine instabilities of immiscible magnetic fluids, the characteristic phenomena of miscible magnetic fluids feature a fading interface between magnetic fluid and diesel. The growth of instabilities is facilitated mainly by increasing the speed of rotation or strengthening the magnetic field. However, magnetic fields provide less facilitation of growth, due to the magnetoviscous effect. At the beginning of the growth process, the magnetic effect is dominant in the magnetization phase because of the strong repulsion of dipoles. Later, rotation becomes the dominant facilitator during the rotation phase, as the radius of the growing drop increases. The growth rate α and Pe_c show a good linear regression relationship, and the results obtained verify the dominance of the rotation effect in the later period. The Coriolis effect is confirmed by the bending phenomena for tiny labyrinthine instabilities along the direction of rotation of the Hele-Shaw cell.

The pressure gradients tend to hinder growth because of their opposing directions, but the effects of these gradients can be reduced by designing a closed-flow rotating Hele-Shaw cell rather than an open-flow cell. In addition, a larger gap depth helps to greatly accelerate the magnetic drop's growth rate by reinforcing the advections induced by both the magnetic field and the rotation. These results validate the view that the Hele-Shaw cell should be considered as a three-dimensional model. Finally, the ratio of the wavelength and the gap depth is investigated, and is found to be around 7 ± 1, which confirms the findings of previous studies. This ratio also remains consistent as Pe_m increases.

ACKNOWLEDGMENTS

The authors would like to offer their thanks for the financial support for this research given by the Research Grants Council, Hong Kong, under Contract No. GRF PolyU 152168/14E.

[1]C. Y. Wen, C. Y. Chen, and S. F. Yang, "Flow visualization of natural convection of magnetic fluid in a rectangular Hele-Shaw cell," J. Magn. Magn. Mater. **252**, 206 (2002).
[2]C. Y. Wen, K. P. Liang, H. Chen, and L. M. Fu, "Numerical analysis of a rapid magnetic microfluidic mixer," Electrophoresis **32**, 3268 (2011).
[3]C. Y. Wen and W. P. Su, "Natural convection of magnetic fluid in a rectangular Hele-Shaw cell," J. Magn. Magn. Mater. **289**, 299 (2005).
[4]C. Y. Wen, C. P. Yeh, C. H. Tsai, and L. M. Fu, "Rapid magnetic microfluidic mixer utilizing AC electromagnetic field," Electrophoresis **30**, 4179 (2009).
[5]R. E. Rosensweig, *Ferrohydrodynamics* (Dover Publications, 1997).
[6]E. Blūms, A. Cebers, and M. M. Maĭorov, *Magnetic Fluids* (Walter de Gruyter, 1997).
[7]M. Igonin and A. Cebers, "Labyrinthine instability of miscible magnetic fluids," Phys. Fluids **15**, 1734 (2003).
[8]C.-Y. Chen and C.-Y. Wen, "Numerical simulations of miscible magnetic flows in a Hele–Shaw cell: Radial flows," J. Magn. Magn. Mater. **252**, 296 (2002).

[9]C.-Y. Chen, "Numerical simulations of fingering instabilities in miscible magnetic fluids in a Hele-Shaw cell and the effects of Korteweg stresses," Phys. Fluids **15**, 1086 (2003).
[10]C.-Y. Chen and Y.-C. Liu, "Numerical simulations of miscible fluids on a rotating Hele–Shaw cell with effects of Coriolis forces," Int. J. Numer. Methods Fluids **48**, 853 (2005).
[11]C.-Y. Chen and H.-J. Wu, "Numerical simulations of interfacial instabilities on a rotating miscible magnetic droplet with effects of Korteweg stresses," Phys. Fluids **17**, 042101 (2005).
[12]C.-Y. Chen, H.-J. Wu, and L. Hsu, "Numerical simulations of labyrinthine instabilities on a miscible elliptical magnetic droplet," J. Magn. Magn. Mater. **289**, 364 (2005).
[13]C.-Y. Wen, C.-Y. Chen, D.-C. Kuan, and S.-Y. Wu, "Labyrinthine instability of a miscible magnetic drop," J. Magn. Magn. Mater. **310**, e1017 (2007).
[14]H. H. Hu and D. D. Joseph, "Miscible displacement in a Hele-Shaw cell," Z. Angew. Math. Phys. **43**, 626 (1992).
[15]C.-Y. Wen, C.-Y. Chen, and D.-C. Kuan, "Experimental studies of labyrinthine instabilities of miscible ferrofluids in a Hele-Shaw cell," Phys. Fluids **19**, 084101 (2007).
[16]G. Kitenbergs, A. Tatulcenkovs, K. Ērglis, O. Petrichenko, R. Perzynski, and A. Cēbers, "Magnetic field driven micro-convection in the Hele-Shaw cell: The Brinkman model and its comparison with experiment," J. Fluid Mech. **774**, 170 (2015).
[17]K. Ērglis, A. Tatulcenkov, G. Kitenbergs, O. Petrichenko, F. Ergin, B. Watz, and A. Cēbers, "Magnetic field driven micro-convection in the Hele-Shaw cell," J. Fluid Mech. **714**, 612 (2013).
[18]S. Waters and L. Cummings, "Coriolis effects in a rotating Hele-Shaw cell," Phys. Fluids **17**, 048101 (2005).
[19]L. W. Schwartz, "Instability and fingering in a rotating Hele–Shaw cell or porous medium," Phys. Fluids A **1**, 167 (1989).
[20]A. G. Emslie, F. T. Bonner, and L. G. Peck, "Flow of a viscous liquid on a rotating disk," J. Appl. Phys. **29**, 858 (1958).
[21]J.-D. Chen, "Radial viscous fingering patterns in Hele-Shaw cells," Exp. Fluids **5**, 363 (1987).
[22]C.-Y. Chen and S.-W. Wang, "Interfacial instabilities of miscible fluids in a rotating Hele–Shaw cell," Fluid Dyn. Res. **30**, 315 (2002).
[23]C.-Y. Chen, Y.-S. Huang, and J. A. Miranda, "Diffuse-interface approach to rotating Hele-Shaw flows," Phys. Rev. E **84**, 046302 (2011).
[24]L. Carrillo, F. Magdaleno, J. Casademunt, and J. Ortín, "Experiments in a rotating Hele-Shaw cell," Phys. Rev. E **54**, 6260 (1996).
[25]E. Álvarez-Lacalle, J. Ortín, and J. Casademunt, "Nonlinear saffman-taylor instability," Phys. Rev. Lett. **92**, 054501 (2004).
[26]E. Alvarez-Lacalle, H. Gadêlha, and J. A. Miranda, "Coriolis effects on fingering patterns under rotation," Phys. Rev. E **78**, 026305 (2008).
[27]Q. Li, Y. Xuan, and J. Wang, "Experimental investigations on transport properties of magnetic fluids," Exp. Therm. Fluid Sci. **30**, 109 (2005).
[28]J. P. McTague, "Magnetoviscosity of magnetic colloids," J. Chem. Phys. **51**, 133 (1969).
[29]S. Odenbach and S. Thurm, *Magnetoviscous Effects in Ferrofluids* (Springer, 2002).
[30]C. Y. Kao, "Study on the interfacial instabilities of miscible ferrofluids in various gap heights Hele-Shaw cells under different incremental rates of external magnetic field," M.Sc. thesis, National Cheng Kung University, Taiwan, 2013.